Chalmers Publication Library

(Article begins on next page)

Linear variable optical filter-based ultraviolet microspectrometer

Arvin Emadi,[1,*] Huaiwen Wu,[1] Ger de Graaf,[1] Peter Enoksson,[2]
Jose Higino Correia,[3] and Reinoud Wolffenbuttel[1]

[1]Faculty of Electrical Engineering, Mathematics and Computer Science, Department of Microelectronics/
Electronic Instrumentation, Delft University of Technology, Mekelweg 4, 2628 CD, Delft, The Netherlands

[2]Micro and Nanosystems, BioNano Systems Laboratory, MC2-Chalmers University of Technology,
SE412 96 Gothenburg, Sweden

[3]Department of Industrial Electronics, Campus Azurem, University of Minho, 4800 Guimaraes, Portugal

*Corresponding author: a.emadi@tudelft.nl

An IC-compatible linear variable optical filter (LVOF) for application in the UV spectral range between 310 and 400 nm has been fabricated using resist reflow and an optimized dry-etching. The LVOF is mounted on the top of a commercially available CMOS camera to result in a UV microspectrometer. A special calibration technique has been employed that is based on an initial spectral measurement on a xenon lamp. The image recorded on the camera during calibration is used in a signal processing algorithm to reconstruct the spectrum of the mercury lamp and the calibration data is subsequently used in UV spectral measurements. Experiments on a fabricated LVOF-based microspectrometer with this calibration approach implemented reveal a spectral resolution of 0.5 nm.   © 2012 Optical Society of America
  OCIS codes: 300.6190, 310.4165, 220.0220, 300.6540.

1. Introduction

Ultraviolet (UV) spectroscopy has many applications in pharmaceutical analysis [1], quantitative analysis of transition metals [2], atmospheric gas sensing [3], and bimolecular identification [4]. Microelectro-mechanical-system-based microspectrometers have huge potential in some of these applications because of the small sample volume required and the fast response [5]. Additional advantages emerge in case the fabrication of the MEMS-based optical microsystem is compatible with silicon integrated circuit (IC) technology. On-chip co-integration of the optical system with integrated circuitry enables in-system data preprocessing in the smallest possible system, the chip. Data storage provides opportunities for improving the user interface and reducing the need for a laboratory with all the logistics associated with such a central infrastructure [6].

Microspectrometers, operating in the UV spectral range, require either a small feature size in the grating design, or an optical resonator design with a cavity width less than 200 nm (when operated in 300–400 nm band). Fabrication and electronic modulation of a resonator with such a narrow air gap between the two mirrors is severely hindered by capillary forces inside of the cavity. Also, electrostatic pull-in and subsequent sticking of the two mirrors limits the operating range of the device to one third of the initial air gap [7,8].

These problems are avoided in UV linear variable optical filters (LVOF) fabricated in post-processing steps after completion of the UV photodetector array and circuits in a standard IC technology [9]. Such an

LVOF-based microspectrometer was reported for the visible spectral range by combining an LVOF with a CMOS camera [10]. In this article, we present the optical design, implementation, and signal processing required for implementing an LVOF microspectrometer in the UV spectral range. The basic idea was presented before in [11].

2. Design and Fabrication of a UV LVOF

Figure 1 shows a tapered Fabry–Perot (FP) type of LVOF. Collimated light is projected on the surface of the LVOF. The light passing through the LVOF is bandpass filtered determined by the width of the local resonator, and thus, by the spatial position along the length of the LVOF [12].

The LVOF is basically a one-dimensional array of many FP type of optical resonators. Rather than a huge number of discrete devices, the LVOF has a center layer (the resonator cavity) in the shape of a strip and a thickness that changes over its length. Dielectric mirrors are on either side. Thus, the narrow passband wavelength of the LVOF varies linearly along its length. A detector array positioned underneath the LVOF is used for recording the spectrum of the incident light.

The UV LVOF is intended to operate in the wavelength range in between 320 and 400 nm. The filter design critically depends on the choice of the materials used for the high-n and low-n layers. The ratio between the indices of refraction should be at maximum, whereas absorption in the materials should be at minimum. A suitable choice for materials in the intended UV spectral range involves HfO_2 and SiO_2 as respectively high-n and low-n materials. Since the optical parameters of these materials do depend on the details of the deposition technique used, the refractive indices have been measured by ellipsometry. Table 1 shows the designed thickness of the layers used for the multilayered LVOF using HfO_2 and SiO_2. Figure 2 shows the measured refractive indices of HfO_2 and SiO_2 in the wavelength range between 280 and 1000 nm. The extinction coefficient in both materials is considered to be negligible for wavelengths above 270 nm. This is in agreement with published optical data of these materials [13]. This is also confirmed by the fact that in our ellipsometry characterizations it was possible to have a very good fit between the ellipsometric data and a lossless Cauchy model of the materials [14].
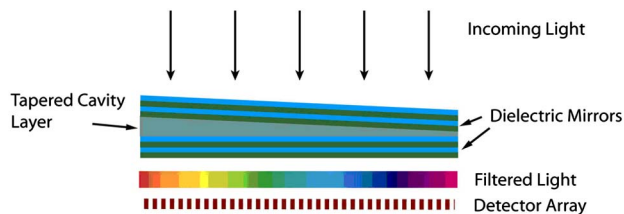
Table 1. Layer Thicknesses of Multilayered UV Linear Variable Filter

Material	Thickness (nm)
HfO_2	43.5
SiO_2/HfO_2	59/43.5
SiO_2/HfO_2	59/43.5
SiO_2/HfO_2	59/43.5
SiO_2/HfO_2	59/43.5
SiO_2	440–600
HfO_2/SiO_2	43.5/59
HfO_2/SiO_2	43.5/59
HfO_2/SiO_2	43.5/59
HfO_2/SiO_2	43.5/59
HfO_2/SiO_2	43.5/59
HfO_2	43.5

The thickness of the tapered cavity layer changes linearly from 440 to 600 nm to cover the spectral range of interest. The spectral response of the filter is simulated using the thin film design simulation software package TFCalc 3.3 [15] and the result is shown in Fig. 3.

It should be noted that the simulations at the designed values of the layers reveals two different wavelengths that are transmitted through the filter at any value of the cavity thickness (any position along the LVOF). These two wavelengths are from different resonance orders and their wavelength separation limits the free spectral range (FSR). Increasing the thickness of the cavity from 440 to 600 nm (as indicted by the curves from bottom to top in Fig. 3) covers the spectral range of 315 to 350 nm in one of the resonance orders, while the other covers the range between 350 and 400 nm.

The maximum reflecting bandwidth of a Bragg reflector, which is the basic element in the structure of the LVOF, can be calculated from Eq. (1), [16,17].

$$\frac{\Delta\lambda}{\lambda_0} = \frac{4}{\pi} \text{Arcsin}\left(\frac{n_2 - n_1}{n_2 + n_1}\right). \tag{1}$$

In which $\Delta\lambda$ is the maximum reflecting bandwidth, λ_0 the reference wavelength, and n_2 and n_1 refractive indices of the dielectric materials. We
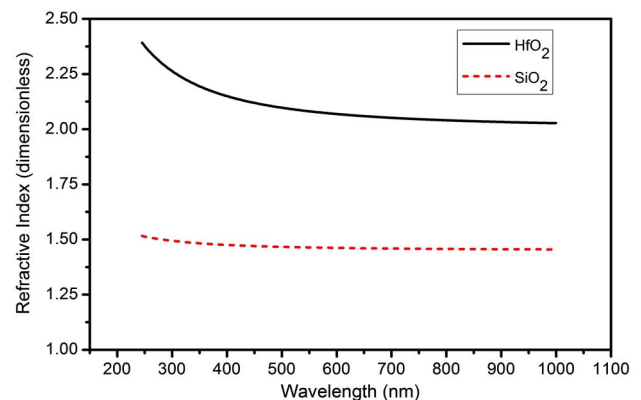

Fig. 1. (Color online) Schematic view of a tapered Fabry–Perot LVOF.

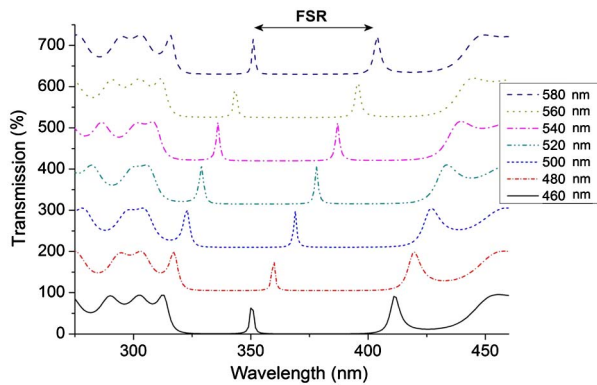Fig. 2. (Color online) Refractive indices of HfO_2 and SiO_2.

Fig. 3. (Color online) Simulated spectrum of the LVOF for different values of the cavity thickness.

would like to emphasize that unlike the FSR, the reflection bandwidth depends only on the dielectric mirror and is a property of the mirror and dielectric materials used.

The maximum value of the FSR, which limits the operation bandwidth of LVOF microspectrometer, is half of the reflection bandwidth, $\Delta\lambda/2$, [17,18]. Increasing the thickness of the cavity layer implies a higher operation mode for the FP structure of the LVOF, which results in higher spectral resolution (smaller FWHM), but a smaller FSR. For HfO_2 and SiO_2 and a reference wavelength of $\lambda_0 = 350$ nm, the maximum stopband of the dielectric mirrors results from Eq. (1) as $\Delta\lambda = 84$ nm. Consequently, the FSR = 42 nm. The transmission at two different resonance orders has been used for optical characterization of the LVOF and the results are shown in Sec. 4. We should note here that the materials used are lossless in the wavelength range of the interest. Otherwise, the loss of the cavity severely reduces the resolution of the FP.

Fabrication involves an IC-compatible reflow process [19]. Figure 4 shows the process flow. Initially, layers 1–10 were sputtered on the substrate (forming the bottom dielectric mirror and the FP cavity). Sputtering of the dielectric layers has been done in the FHR MS 150 sputtering machine. It is possible to achieve an optical thickness variation of the layers less than 2%. Figure 5 shows the thickness variations of sputtered SiO_2 over 69 points on a 6 in. (150 mm) wafer. The thicknesses were measured by ellipsometry at 69 points on the wafer. For SiO_2, the thickness variation over a 6 in. wafer area is 113.05 ± 2.55 nm or $\pm 2.2\%$ thickness variation. When only the smaller 4 in. (100 mm) inner area is considered, it would result in 112.5 to 115.6 nm thickness
values or 114.05 nm ± 1.55 nm, which implies a $\pm 1.36\%$ thickness variation. We similarly found the thickness variations for HfO2 to be less than 2%.

Photoresist was spin-coated and patterned by a special pattern optimized to produce a constant slope (linearly varying thickness) after reflow. The thickness profile of the tapered resist structures were characterized by a stylus profilometer [19]. The
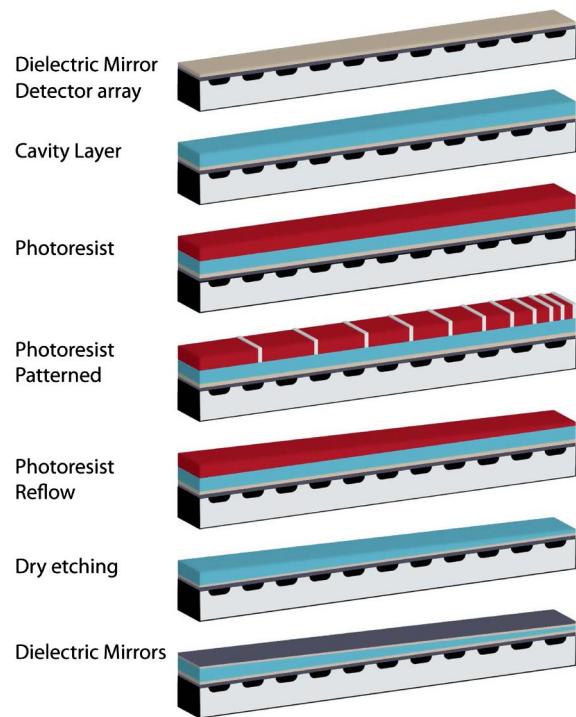

Fig. 4. (Color online) Process flow for fabrication of LVOFs.

tapered resist pattern was transferred into a SiO_2 cavity layer by a dry-etching process that was optimized for minimum surface roughness. The main important thing in the dry-etching process was to operate in the lowest possible chamber pressure to avoid nanomasking which causes the rough surface after the dry-etching [20]. An Oxford plasmalab induced coupled plasma reactive ion etcher tool was used for the process. It was possible to etch with a minimum chamber pressure of 6 mTorr. Although operating in low chamber pressure slows down the etching process, surface roughness is strongly reduced. The gases used for the process were NF_3 5 sccm, CHF_3 5 sccm, O_2 20 sccm, and Ar 50 sccm. At 100 W RF power an etch rate of 14 nm/min is obtained for SiO_2 and 65 nm/min for the resist. Thus, the selectivity of resist/SiO_2 is 4.6. The high selectivity is important in an UV LVOF because very small
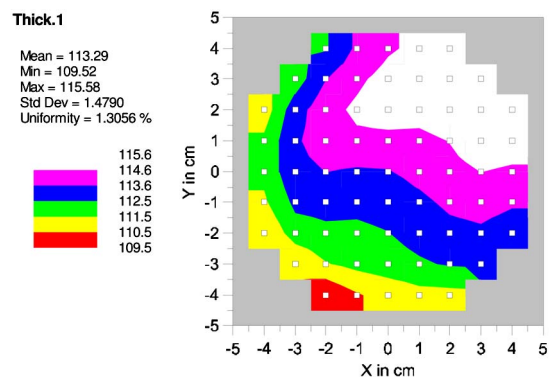

Fig. 5. (Color online) Thickness variation of sputtered SiO_2 over a 6 in. wafer, all values in nanometers.
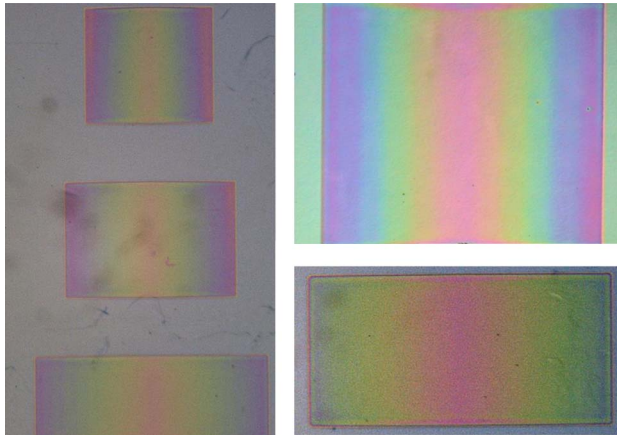
Fig. 6. (Color online) Photograph of UV LVOFs fabricated on glass substrates.

slopes are required (about 100 nm thickness variation along the length of the LVOF). This selectivity makes it possible to initially have a higher slope in the resist, while reducing the slope after dry-etching. CHF_3 can be used instead of the NF_3 in case lower selectivity would be required.

Figure 6 shows a photograph of the fabricated UV LVOFs. The rainbow pattern on the LVOFs is the result of the slope of the structures. The IC-compatible process for fabrication of the tapered layers allows the possibility for fabrication of devices with different values of fixed slope with one lithography step. Because of smaller wavelength in the UV spectrum, as compared to visible spectra, the roughness is more critical in the UV spectral range. The roughness of the surface of the fabricated devices was measured by ellipsometry [21,22]. Results show a roughness of 4 nm.

As it can be noted from the photograph of the fabricated UV LVOFs, there are two identical LVOFs in one hill-shaped structure. The initial idea behind the mask design was to use the data from both the identical LVOFs on the sides. This was expected to be helpful, for example, in case the light on the LVOF is not properly collimated. However, during experimentation it was found that this information is not useful when also considering the data processing on the actual measurements.
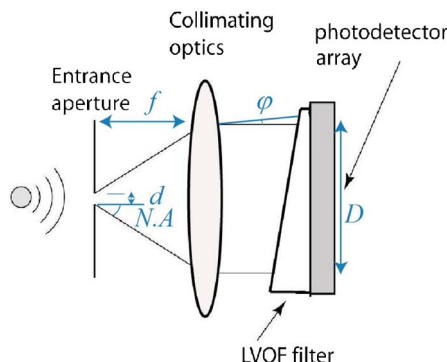

Fig. 7. (Color online) Structure of an LVOF microspectrometer.

The structure of an LVOF-based microspectrometer is shown in Fig. 7. Light passes an aperture and collimating optics before being projected onto the LVOF, which is placed or deposited on the top of the detector.

From Fig. 7 it can be found: $f = D/2NA$, in which D is the length of the LVOF, f is the focal length of the lens, and NA is entrance numerical aperture. The Smith–Helmholtz invariant theorem [23] results in $d \times NA = D \times \varphi$, which can be rewritten as: $d = D \times \varphi/NA$. In which, d is the diameter of the aperture and φ is the maximum acceptable angle of incidence on the LVOF. The diameter of the aperture, d, depends on the maximum acceptable angle of incident on the LVOF, φ. Therefore, any specified maximum value for φ results in a maximum value for d. The transmission through the LVOF is simulated for this purpose for several values of the angle of incidence and at a wavelength at the center of the operating bandwidth of the LVOF. The result is shown in Fig. 8, which indicates that a 5° deviation from the normal incident the spectral peak of transmission results in a spectral shift over 0.4 nm, approximately. Therefore, the angle of incidence is limited to $\varphi_{max} = 5°$ for a maximum spectral inaccuracy of 0.5 nm. The value $\varphi = 5°$ is inserted in $d = D \times \varphi/NA$. Considering an LVOF with a length of 5 mm and assuming NA = 0.25 results in $f = D/2NA = 10$ mm for the focal length of collimating optics. The aperture size is calculated as mentioned and yields: $d = D\varphi/NA = 5$ mm $\times 5°/0.25$ rad ≈ 1.7 mm. This determines the maximum value of the aperture size, d. Therefore, the aperture size in an LVOF-based system is limited by the acceptable spectral shift. A further reduction of aperture improves spectral accuracy at the expense of optical throughput: the amount of light entering the optical system would decrease.

Collimating optics has been designed and implemented in a C-mount holder that is put on the top of the CMOS camera. Although a C-mount holder is relatively bulky, it is a convenient solution when
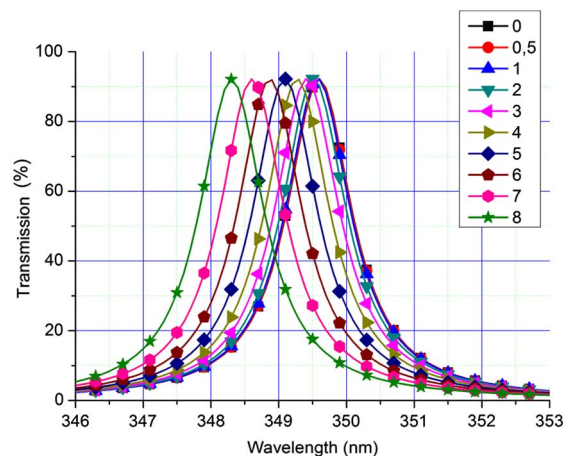

Fig. 8. (Color online) Transmission through a Fabry–Perot resonator at different angles in degrees.

parameters of collimating optics need to be changed for different experiments. In a final microspectrometer design the C-mount holder has to be replaced with a miniaturized version.

3. Characterization and Calibration of UV LVOF

Collimated monochromatic light has been projected on the LVOF mounted on the CMOS camera. The wavelength of the projected light changes from 320 to 400 nm with 0.5 nm steps, using a programmed monochromator with results in 161 spectral channels. Figure 9 shows the recorded image on the LVOF spectrometer for different wavelengths in the range from 315 to 400 nm. We can see the reoccurrence of illuminated regions on the images at an increment of about 40 nm. This is due to the 42 nm FSR as explained previously. The recorded intensity profile on the camera pixels is normalized at each wavelength by dividing it to the measured camera responsivity.

Figure 10 shows the normalized recorded intensity profile of the CMOS camera pixels at different wavelengths. Due to the 42 nm FSR of the LVOF and the resulting occurrence of illuminated regions on the camera with 42 nm steps, two separate sets of curves are plotted, each covering a 40 nm bandwidth. The curves are plotted with 2 nm wavelength increments. The measurements show a 4 pixels/nm shift in the position of the illuminated regions on the camera shown in Fig. 11. Figure 11 shows a zoomed in portion of Fig. 10 for better illustration. The half-power line width (HPLW) of illuminated regions equals to 9 pixels, which is equivalent to 54 μm spatially and 1.2 nm in terms of resolution.

The measured intensity profile recorded by the camera at each wavelength using this monochromator scan is imported (without normalization) into a signal processing algorithm to result in the LVOF microspectrometer calibration matrix, which can subsequently be used for calculation of any spectrum
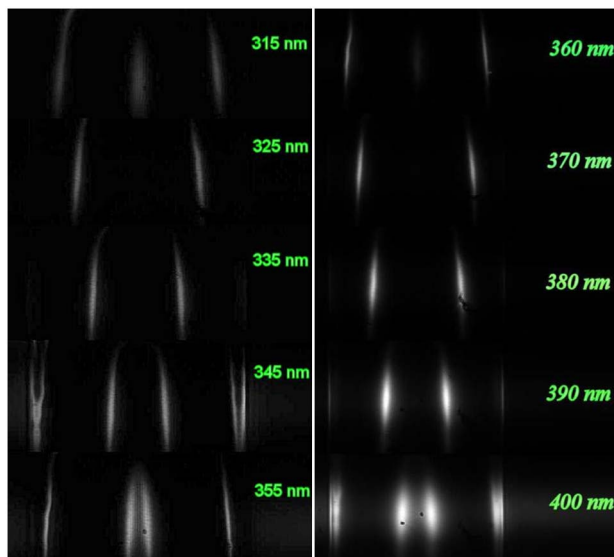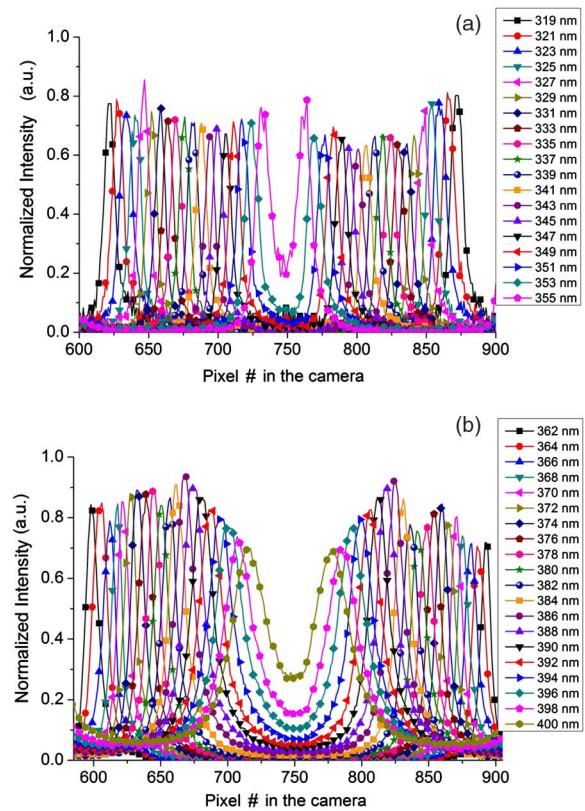

Fig. 10. (Color online) Normalized recorded intensity on the LVOF spectrometer for the 315 to 400 nm wavelength region.

incident on the UV LVOF. The signal processing required is similar to that described in [24] and presented for a visible LVOF microspectrometer in [10]. The technique is summarized here.

Let us assume the spectral bandwidth of interest is divided into N spectral channels and there exists N spectrally different (independent) detectors. The element C_{ij} in matrix C is defined as the intensity of channel i of the detector to component j in the spectrum ($i,j = 1...N$). The matrix C can be directly constructed from the data of a calibration measurement process. The maximum value of N is the number of the pixels on the camera, but can be limited

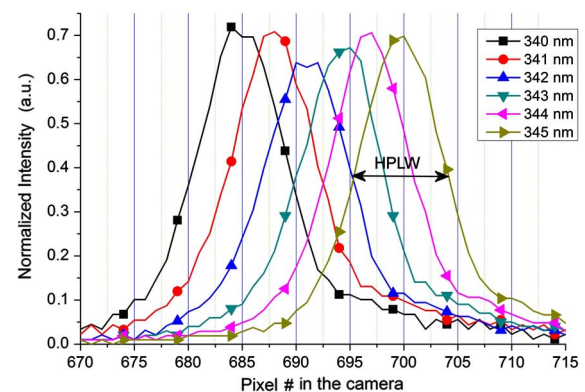Fig. 9. (Color online) Recorded image at several wavelengths.

Fig. 11. (Color online) Zoomed in portion of the figure of normalized recorded intensity.

by the spectral capability of the calibrating instrument (a monochromator). Hence, the measured intensity on the detector channels can be described as

$$D_{1N} = C_{NN} \cdot I_{1N} \qquad (2)$$

in which d_i denotes the measured intensity in channel i and I_i denotes the input spectrum intensity in channel i that has to be calculated. In other words, matrix D_{1N} is the raw data recorded on the camera pixels, matrix I_{1N} is the spectrum of light that has to be calculated and matrix C_{NN} is the calibration matrix, which is determined during the calibration process. In the calibration process, the light from a broadband source (xenon lamp) is filtered by a monochromator and the selected wavelength is varied in the spectral range of interest for all the N spectral channels. For each spectral channel from the above equations, calibration is equivalent to deliberately having: $I = [0, 0, ...0, I_m = 1, 0, ...0]$ when channel m is selected from the monochromator. In this case the recorded intensities on the pixels give the values of column m of the C matrix: $D_{1N} = C_{NN} \cdot I_{1N} = [c_{lm}, c_{lm}, ..., c_{Nm}]$.

Repeating the procedure for all the N spectral channels, results in determination of C_{NN} matrix. For a properly designed and fabricated LVOF, matrix C has no singularity and it is possible to take the inverse transform of the matrix. Therefore, matrix I can be calculated as $I_{1N} = C_{NN}^{-1} \cdot D_{1N}$. However, since the measured matrix D is added with noise the above solution does not give the best answer. The sources of the disturbance (or noise) in the measured raw data include primarily insufficient collimation, out of the band signal, and errors in the estimation of the calibration matrix (due to inaccuracy in the monochromator instrument). If the disturbance in the system is not negligible as compared to the signal (low SNR) the above approach would result in negative values in some spectral channels, which is not physically acceptable. An iterative procedure needs to be implemented to calculate the matrix I by minimizing matrix E:

$$E = D_{1N} - C_{NN} \cdot \hat{I}_{1N}, \qquad (3)$$

in which matrix $\hat{I}_{NN}$ is the estimate of I. The least mean square (LMS) algorithm is implemented based on the following equations:

$$E_n = d - C \cdot \hat{I}_n$$
$$\hat{I}_{n+1} = \hat{I}_n + \mu C \cdot E_n. \qquad (4)$$

E_n denotes the error and $\hat{I}_n$ the estimate of the spectrum at each recursive step and μ the convergence coefficient. A higher value for μ results in faster convergence of the algorithm. However, it can also result in divergence (i.e., instability) of the algorithm. The goal of the algorithm is to decrease the mean square of E_n at each step. This results in
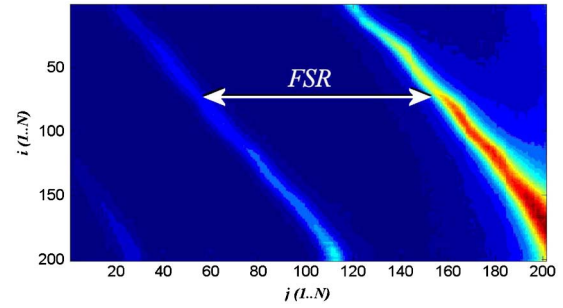

Fig. 12. (Color online) Surface plot of the calibration matrix of the UV LVOF.

the best possible estimate for the spectrum vector $\hat{I}$. The value of E_n remains non-zero due to noise and disturbances in the measurements.

4. Spectral Measurements

This LVOF-based microspectrometer is intended for use in the spectral band in between 310 and 400 nm. The total number of channels is 201 each 0.5 nm wide. The data from the calibration measurement (characterization) is imported into the signal processing algorithm to construct the calibration matrix, C_{NN}, as introduced in the previous section. Figure 12 shows a 2D plot of the values in the 201 × 201 calibration matrix, which is formed for the UV LVOF. The x axis on the plot presents different wavelength channels and the y axis presents the channels or pixels on the detector array. From the rows on the plot we can note the FSR of the LVOF. Parallel lines demonstrate the linear movement of the illuminated regions on the LVOF when linearly increasing the wavelength within the operating bandwidth. We can also see the widening of the illuminated regions (due to widening of the spectral peaks) when the wavelength gets closer to 400 nm for spectral channels 160 to 200. Furthermore, it is possible to see the decreasing response at shorter wavelengths.

The objective is to measure the spectrum of a mercury lamp in the UV spectral range. The mercury lamp has a high intensity in this spectral range and demonstrates a unique spectrum. The result is
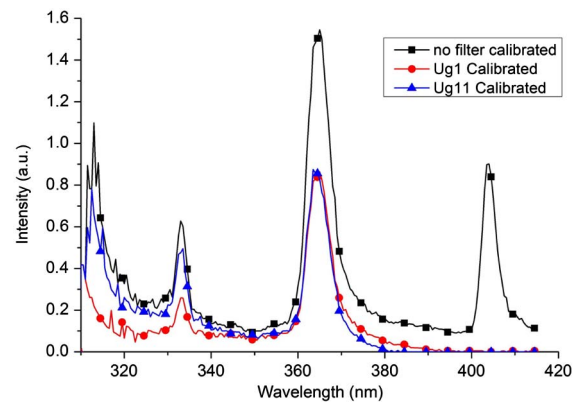

Fig. 13. (Color online) Measured spectrum of the mercury lamp, including the effect of the UG1 and UG11 filters.
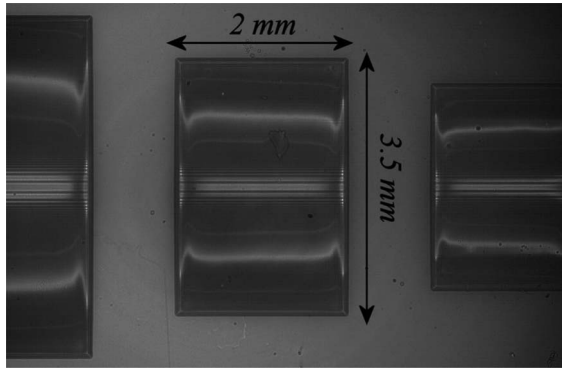
Fig. 14. Image recorded by the UV LVOF microspectrometer when illuminated by a mercury lamp.

Fig. 16. (Color online) Result of spectral calculation for 320 to 380 nm spectral range.

shown in Fig. 13. Two Schott glass filters, types Ug1 and Ug11, have been used to eliminate the unwanted part of the spectrum. Ug1 has a passband in 300–400 nm spectral range and Ug11 has the passband in between 250 and 390 nm. As is shown from the measurement with Ug11, the spectrum for wavelength longer than 380 nm is eliminated. Therefore, in our measurements with LVOF we have used the Ug1 filter to selectively remove the unwanted part of the spectrum.

Figure 14 shows the recorded image on the LVOF camera when illuminated by the mercury lamp. The image shows three UV LVOFs with different sizes and slopes. We can note the distortions of the bright spectral lines at the sides of the structures, which are due to the reflow process step in the fabrication. This can be prevented in an optimized process. Moreover, data from these parts of the LVOF are neglected in the further calculations. The spectral peaks can be readily identified from the image.

The data from the image is imported to the signal processing algorithm to extract the spectrum. Figure 15 shows a comparison between the spectrum after applying the algorithm and the measurement with a TRIAX 180 monochromator.

The entire spectral range of the LVOF, 320 to 415 nm, has been used in this spectral calculation. From the comparison we can note an extra spectral
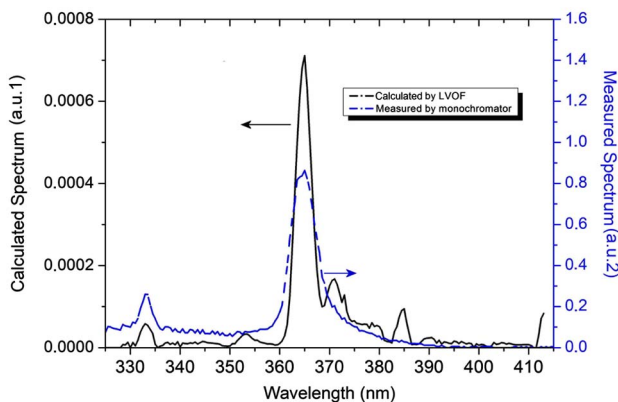
peak predicted by signal processing algorithm at 385 nm, which is not present in the measurement with the monochromator. This peak is due to folding from peak in a band higher than the FSR range of the LVOF. The actual peak of the mercury lamp at 334 nm has been correctly identified. It can be noted from Fig. 10 that the position of the peak at 334 nm is equal to the position of the peak at 386 nm. These are two different wavelength peaks from different resonance orders of the cavity. The LMS signal processing algorithm was not able to make a difference between these two and has divided the signal level that was recorded on the camera at that position between both of the resonant orders. The main conclusion that can be drawn from this result is that it is essential to limit the measurement bandwidth to the FSR. The other characteristic difference in the measured spectrums is the lower calculated baseline of spectral power in the calculated spectrum.

In a second attempt the spectral band in the signal processing algorithm is limited to 325 to 380 nm. Figure 16 shows the result.

In both calculations the spectral response of the CMOS pixels was taken into account. The spectrum calculated for the narrower bandwidth has better agreement with the measurement with the monochromator. In both cases the low sensitivity of the CMOS camera in the UV leads to an increased noise level. However, the effect is more pronounced in the wideband application due to the fact that the noise and disturbances limits the ability of the algorithm to distinguish between the two possible wavelengths for each pixel. This results in additional peaks appearing in the reconstructed spectrum. Detector arrays with high sensitivity in the UV spectral range need to be applied to improve the calculations. The result demonstrates that the LMS signal processing technique is suitable for measurements in the case of a continuous spectrum, as is the case of a mercury lamp. The suitability of the LMS algorithm for a spectrum with discrete features was shown in [10] for an LVOF microspectrometer operating in the visible spectrum by measuring the spectrum of a neon lamp.

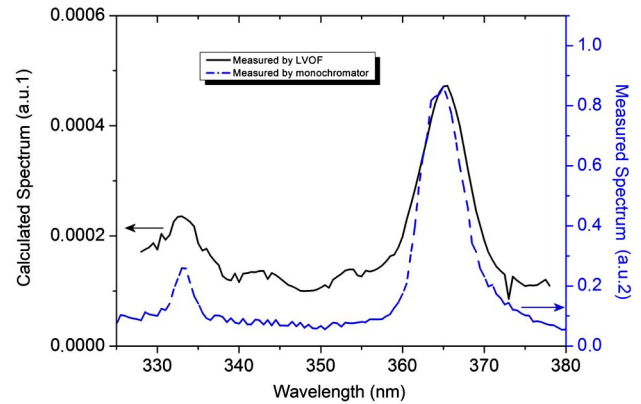Fig. 15. (Color online) Calculated spectrum from the LVOF compared with measurement by a monochromator.

5. Conclusions

The design and implementation of an LVOF-based microspectrometer for operation in the UV spectral range is presented in this article. The IC-compatible fabrication enables a very compact and rigid microspectrometer system.

The strength of the LVOF-based microspectrometer concept is the high resolving power in a relatively narrow band, which makes it particularly suitable in applications where the spectral analysis around an absorption or emission peak is required, such as in fluorescence. The designed operating range is between 320 and 415 nm. The spectral resolution of the basic microspectrometer is significantly improved by using signal processing to calculate the spectrum of light recorded by the image detector. The spectral resolution of the realized UV LVOF is about 1.5 nm and is improved to 0.5 nm after application of signal processing. The spectral measurements show that in order to have unambiguous spectral measurement results with an LVOF spectrometer, the operating bandwidth of the spectrometer should be limited to the FSR of the LVOF.

First prototypes are bulky because of the C-mount. However, the essential optical path is only 10 mm × 5 mm. The most significant limitation at this stage is the low sensitivity of the diodes in the imager in the UV part of the spectrum. The system will be further miniaturized by direct deposition of the LVOF on a customized CMOS imager that is sensitive in the UV range. Collimating optics also need to be miniaturized. The design procedure, fabrication, and signal processing of the UV LVOF remain the same.

References

1. A. Villarisu, M. Fresta, N. Micali, and G. Puglisi, "Potential application of UV reflection spectroscopy on solid pharmaceutical formulation analysis," Int. J. Pharm. **127**, 185–189 (1996).
2. A. J. Merer, "Spectroscopy of the diatomic 3d transition metal oxides," Annu. Rev. Phys. Chem. **40**, 407–438 (1989).
3. F. Z. Chen, D. L. Judge, C. Y. R. Wu, and J. Caldwell, "Low and room temperature photoabsorption cross sections of NH3 in the UV region," Planet. Space Sci. **47**, 261–266 (1998).
4. A. Rodger and K. Sanders, "Biomacromolecular applications of UV-visible absorption spectroscopy," in *Encyclopedia of Spectroscopy and Spectrometry*, J. Lindon, ed. (Oxford, 1999), pp. 130–139.
5. R. F. Wolffenbuttel, "MEMS-based optical mini and micro-spectrometers for the visible and infrared spectral range," J. Micromech. Microeng. **15**, S145–S152.
6. G. Minas, R. F. Wolffenbuttel, and J. H. Correia, "A lab-on-a-chip for spectrophotometric analysis of biological fluids," Lab Chip **5**, 1303–1309 (2005).
7. L. Mol, L. A. Rocha, E. Cretu, and R. F. Wolffenbuttel, "Squeezed film damping measurements on a parallel-plate MEMS in the free molecule regime," J. Micromech. Microeng. **19**, 074021 (2009).
8. J. H. Correia, A. Emadi, and R. F. Wolffenbuttel, "UV band-pass optical filter for microspectrometers," ECS Trans. **4**, 141–147 (2007).
9. O. Schmidt, P. Kiesel, and M. Bassler, "Performance of chip-size wavelength detectors," Opt. Express **15**, 9701–9706 (2007).
10. A. Emadi, H. Wu, G. De Graaf, and R. F. Wolffenbuttel, "Design and implementation of a sub-nm resolution micro-spectrometer based on a linear-variable optical filter," Opt. Express **20**, 489–507 (2012).
11. A. Emadi, H. Wu, G. de Graaf, K. Hedsten, P. Enoksson, J. H. Correia, and R. F. Wolffenbuttel, "An UV linear variable optical filter-based micro-spectrometer," Procedia Eng. **5**, 416–419 (2010).
12. R. McLeod and T. Honda, "Improving the spectral resolution of wedged etalons and linear variable filters with incidence angle," Opt. Lett. **30**, 2647–2649 (2005).
13. R. Thielsch, A. Gatto, J. Heber, and N. Kaiser, "A comparative study of the UV optical and structural properties of SiO_2, Al_2O_3, and HfO_2 single layers deposited by reactive evaporation, ion-assisted deposition and plasma ion-assisted deposition," Thin Sol. Films **40**, 86–93 (2002).
14. H. G. Tompkins and E. A. Irene, *Handbook of Ellipsometry* (William Andrew Publishing, 2005).
15. TFCalc thin film design software website, http://www.sspectra.com/.
16. J. H. Apfel, "Phase retardance of periodic multilayer mirrors," Appl. Opt. **21**, 733–738 (1982).
17. D. I. Babic and S. W. Corzine, "Analytic expressions for the reflection delay, penetration depth, and absorptance of quarter-wave dielectric mirrors," IEEE J. Quantum Electron. **28**, 514–524 (1992).
18. A. Emadi, "Linear-variable optical filters for microspectrometer application," Ph.D. thesis (Technical University of Delft, 2010).
19. A. Emadi, H. Wu, S. Grabarnik, G. de Graaf, and R. F. Wolffenbuttel, "Vertically tapered layers for optical applications fabricated using resist reflow," J. Micromech. Microeng. **19**, 074014 (2009).
20. K. Mohamed and M. M. Alkaisi, "Three-dimensional pattern transfer on quartz substrates," Microelectron. Eng. **87**, 1463–1466 (2010).
21. J. R. Blanco, P. J. McMarr, and K. Vedam, "Roughness measurements by spectroscopic ellipsometry," Appl. Opt. **24**, 3773–3779 (1985).
22. S. F. Nee, "Ellipsometric analysis for surface roughness and texture," Appl. Opt. **27**, 2819–2831 (1988).
23. M. Born and E. Wolf, *Principles of Optics: Electromagnetic Theory of Propagation, Interference and Diffraction of Light*, 7th ed. (Cambridge University, 1999).
24. D. Massicotte, R. Z. Morawski, and A. Barwicz, "Kalman-filter-based algorithms of spectrometric data correction-Part I: an iterative algorithm of deconvolution, instrumentation and measurement," IEEE Trans. Instrum. Meas. **46**, 678–684 (1997).